Original Paper

Global Optimization for Delineation of Self-potential Anomaly of a 2D Inclined Plate

Khushwant Rao,[1] Shraddha Jain,[1] and Arkoprovo Biswas ●[1,2]

A fast and efficient technique for explanation of self-potential anomalies is of immense importance for exploration, engineering, and environmental problems. Estimation of model parameters of ore bodies in the subsurface is the primary concern in mineral exploration. In most cases, self-potential data are delineated considering various simple or idealized structures for the interpretation of lateral and vertical variations of subsurface ore bodies. In this context, we developed an inversion algorithm to determine the different parameters associated with a 2D inclined plate-type structure, which does not require any a priori information. The developed algorithm can interpret appropriately every parameter with minimum uncertainty. The position of causative source body (x_0), its half-width (w) and its depth (z) were the parameters interpreted using the developed algorithm. It was found that these parameters were well resolved within the estimated uncertainty, although solutions for w showed wide variability. The technique was verified with synthetic data without noise and with different degrees of Gaussian noise. The technique was also confirmed with three field datasets for mineral exploration, and the interpreted parameters were in fair agreement with those reported in earlier works.

KEY WORDS: Self-potential, 2D plate, VFSA, Mineral exploration.

INTRODUCTION

Self-potential (SP) is a passive geophysical technique that measures naturally occurring electric potentials, which are generated in the Earth's surface due to different mechanisms (electrokinetic, electrochemical, thermoelectric and mineralization potential). The method was introduced to decipher the formation of mineralization potential principally linked to sulfide and graphite ore structure (Sato and Mooney 1960; Sundararajan et al. 1998; Mendonca 2008) within the subsurface and it was later used for oxide ore deposits as well (Biswas and Sharma 2014a, 2016). The method has varied applications apart from mineral exploration. It has been extensively applied in engineering problems, hydrogeological surveys, environmental contaminant monitoring, and tracing shear zones (Kulessa et al. 2003; Jardani et al. 2008; Mendonca 2008; Mehanee 2014, 2015; Gobashy et al. 2020). A review of different applications of SP data can be found in Biswas (2017).

Numerous quantitative interpretation techniques for SP data have been developed in the past considering two different categories (Mehanee et al. 2011; Mehanee 2015; Essa and El-Hussein 2017). The first category corresponds to 2D and/or 3D subsurface geologic structures with arbitrary shape and size. The second category is based on idealized buried structures, which can be understood assuming

[1]Department of Geology, Centre of Advanced Study, Institute of Science, Banaras Hindu University, Varanasi 221005, India.
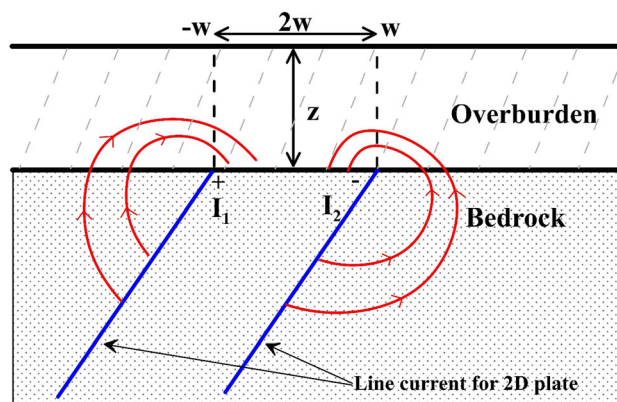[2]To whom correspondence should be addressed; e-mail: arkoprovo@gmail.com

Figure 1. A 2D inclined plate-type structure within the subsurface
(after Mehanee et al. 2011).

simple geometrical shapes such as a sphere, cylinder, fault, and thick sheet. The detail of these categories can be seen in few publications (e.g., Mehanee et al. 2011; Mehanee 2015; Essa and El-Hussein 2017; Abdelrahman et al. 2019). The concern of this present work is that, in some geological settings, there can be a single polarized body that can be interpreted individually (Asfahani and Tlas 2005). In such case, a technique of the second category, with high computational facilities, can be used to interpret the SP anomaly from a single polarized body that does not need a priori data nearby the subsurface geology of that area.

In the past, several approaches have been developed and applied to infer SP anomalies formed due to simple geometrical structures. For example, 2D inclined sheet-type structures have been interpreted by various workers (Paul 1965; Rao et al. 1982; Murthy and Haricharan 1985; Sundararajan et al. 1990, 1998; Jagannadha et al. 1993; Abdelrahman et al. 2003; Murthy et al. 2005; El-Kaliouby and Al-Garani 2009; Monteiro Santos 2010; Essa 2011; Roudsari and Beitollahi 2013; Sharma and Biswas 2013; Biswas and Sharma 2014a, b; Biswas 2016, 2019; Gobashy et al. 2020). Spherical- and cylindrical-type structures have also been interpreted (Paul et al. 1965; Rao et al. 1970; Roy and Mohan 1984; Murthy and Haricharan 1985; Abdelrahman and Sharafeldin 1997; Tlas and Asfahani 2007; Essa et al. 2008; Göktürkler and Balkaya 2012; Tlas and Asfahani 2013; Biswas and Sharma 2015; Mehanee 2015; Roudsari and Beitollahi 2015; Di Maio et al. 2016aa, b; Abdelrahman et al. 2019; Abdelazeem et al. 2019). Moreover, 2D inclined

thick sheet-like bodies have been elucidated by Dmitriev (2012) and later by Biswas and Sharma (2017). A comprehensive review of different interpretation approaches developed for specific subsurface structures can be found in Murthy and Haricharan (1985), Sundararajan et al. 1998, and Biswas (2013). However, in the case of 2D inclined plate-type structures, very few works have been carried out in the past. Hafez (2005) developed a technique for interpreting SP anomaly using first-order moving filters specifically for a short profile. Mehanee et al. (2011) developed a second moving average method for interpreting SP anomalies, which can sufficiently eliminate the SP effect of deeper subsurface structure. Essa and El-Hussein (2017) developed a technique constructed on second horizontal gradient, which can eliminate undesirable anomaly from measured SP anomalies.

In the present work, we encompass the work of Hafez (2005) and Mehanee et al. (2011) as well as the interpretation method of Essa and El-Hussein (2017) for the delineation of 2D plate-type structure for SP anomaly using the forward formula of Lile (1994) and Abdelrahman et al. (1998). As mentioned by Mehanee et al. (2011), there is a need for an effective interpretation of current flow lines, depth, and width of the plate-type structure. Hence, the present work is focused on the interpretation of all parameters associated with plate-type structures. To interpret effectively the SP responses from subsurface mineralized bodies, we used the very fast simulated annealing (VFSA) algorithm intended for the delineation of SP anomaly. We choose this nonlinear global optimization inversion for this
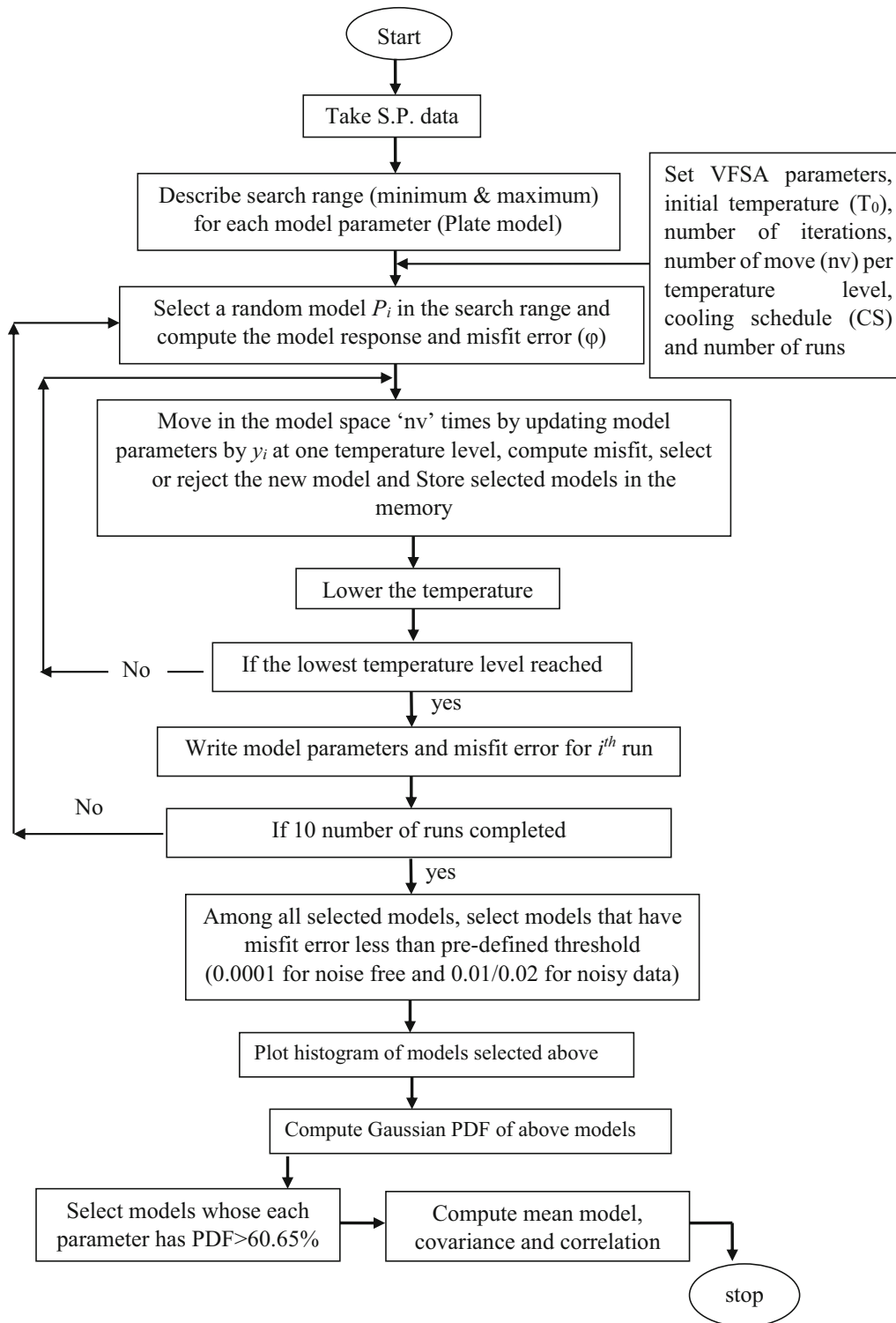
```
                              ┌─────────┐
                              │  Start  │
                              └─────────┘
                                   │
                         ┌───────────────────┐
                         │   Take S.P. data  │
                         └───────────────────┘
                                   │
```

Describe search range (minimum & maximum) for each model parameter (Plate model)

Set VFSA parameters, initial temperature (T₀), number of iterations, number of move (nv) per temperature level, cooling schedule (CS) and number of runs

Select a random model P_i in the search range and compute the model response and misfit error (φ)

Move in the model space 'nv' times by updating model parameters by y_i at one temperature level, compute misfit, select or reject the new model and Store selected models in the memory

Lower the temperature

If the lowest temperature level reached

No

yes

Write model parameters and misfit error for i^{th} run

No

If 10 number of runs completed

yes

Among all selected models, select models that have misfit error less than pre-defined threshold (0.0001 for noise free and 0.01/0.02 for noisy data)

Plot histogram of models selected above

Compute Gaussian PDF of above models

Select models whose each parameter has PDF>60.65%

Compute mean model, covariance and correlation

stop

Figure 2. Flowchart of the inversion process (after Biswas 2013).

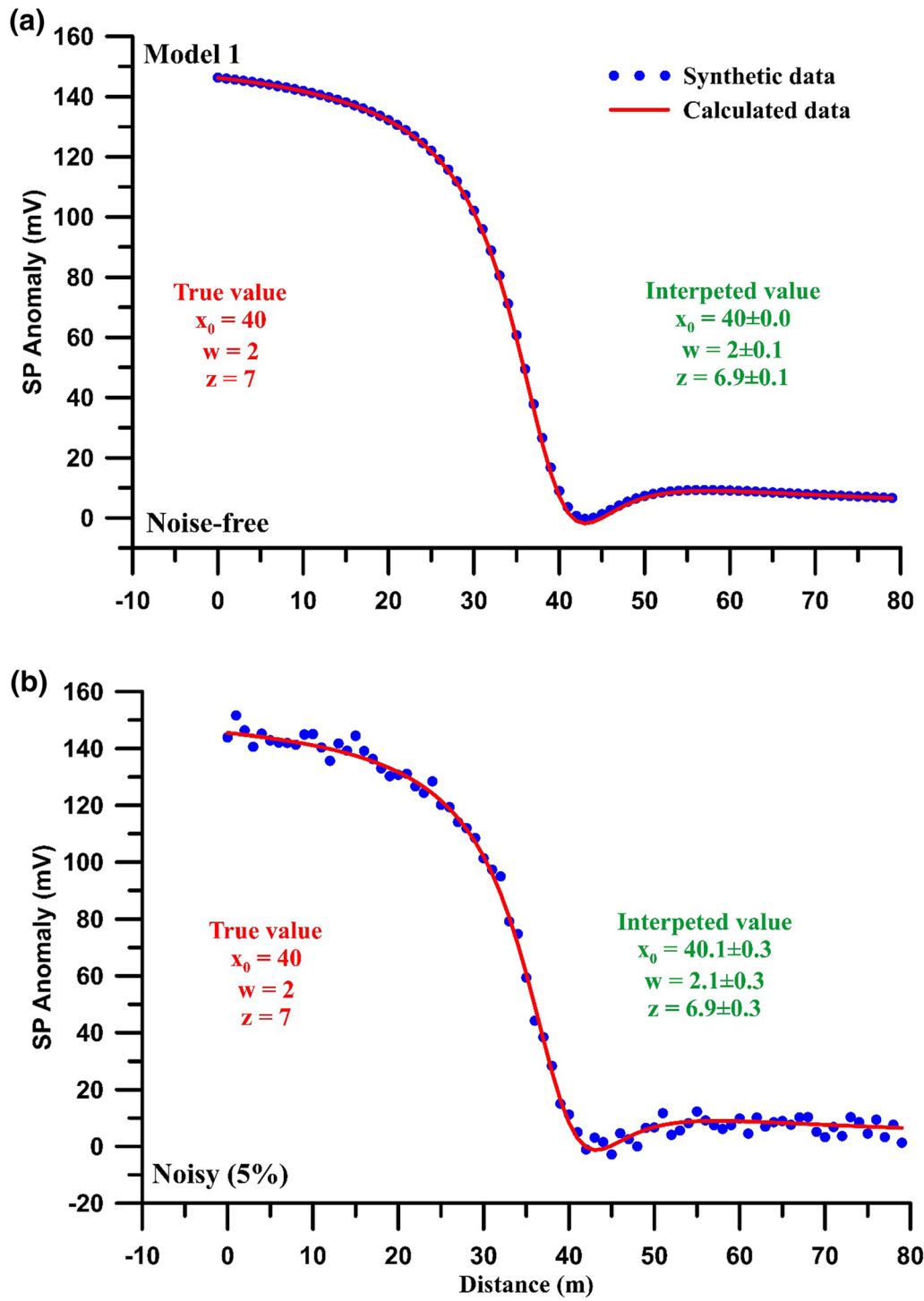**Figure 3.** Computed response for model 1.

Table 1. Computed parameters for model 1

Parameters	True value	Range	Mean model	
			Noise-free	Noisy
I_1	150	0–200	150.3 ± 9.6	139.0 ± 19.6
I_2	100	0–150	100.3 ± 9.7	89.4 ± 19.6
$x_0\ (m)$	40	0–80	40.0 ± 0.0	40.1 ± 0.3
$w\ (m)$	2	0–3	2.0 ± 0.1	2.1 ± 0.3
$z\ (m)$	7	0–10	6.9 ± 0.1	6.9 ± 0.3
Error			2.0×10^{-8}	8.0×10^{-4}
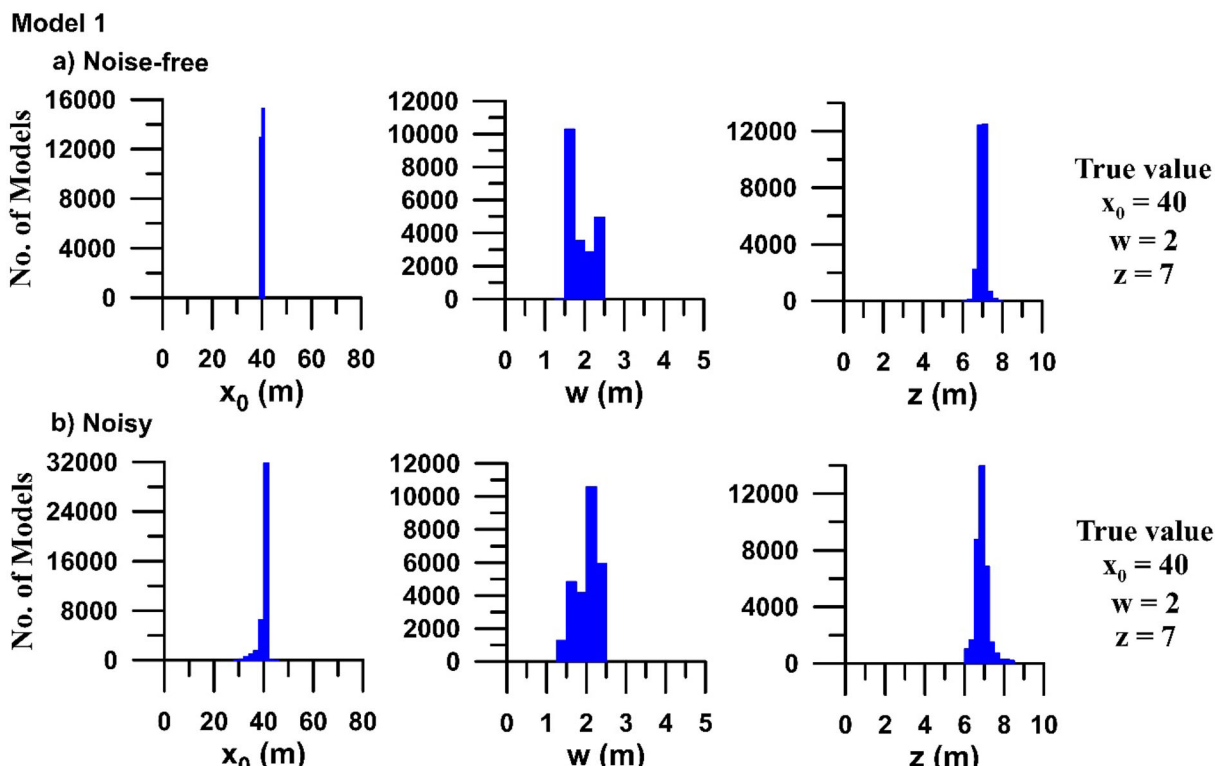
Figure 4. Histogram analysis for model 1.

study because long SP anomalies are mostly non-linear. The inversion algorithm does not require a priori information for the interpretation of SP data. The benefit of this inversion algorithm is that it can interpret effectively short and long profile data, single as well as multiple structures, and it can determine precisely parameters from shallow and deeper structures. The method is exemplified and analyzed on noise-free and noisy synthetic examples, and trialed to elucidate three field anomalies for exploration.

METHODOLOGY

Forward Formulation

Self-potential for a 2D inclined plate (Fig. 1) is given by (Lile 1994; Abdelrahman et al. 1998):

$$V(x) = \frac{\pi}{2}(I_1 - I_2) - I_1 \tan^{-1}\left(\frac{x + w}{z}\right)$$
$$+ I_2 \tan^{-1}\left(\frac{x - w}{z}\right) \tag{1}$$

where z is depth, w is half-width of the body, x is location of the body on the surface, I_1 and I_2 are line currents (Fig. 1). An inclined plate ($I_1 > I_2$) will show an asymmetrical anomaly, while a vertical plate ($I_1 = I_2$) produces a symmetrical anomaly curve.

Global Optimization

The present global optimization is a modified form of simulated annealing (SA), i.e., VFSA, which was derived from the analogy of heat bath algorithm (Sen and Stoffa 2013) and was applied extensively in interpreting various geophysical data. Details of the VFSA can be found in many publications (Rothman 1985, 1986; Sharma 2012; Sen and Stoffa 2013; Sharma and Biswas 2013) and are not briefed here for brevity. It was developed to overcome the limitations of linear inversion and, because of its stability and robustness, it can negate the problem of non-uniqueness and resolution. The other advantages of this inversion method are that it takes less time in computing a large set of data and in finding a global solution (Sen and Stoffa 2013). Moreover, it is quite efficient with minimum CPU time and it takes a lesser amount of memory and with high resolution (Ingber and Rosen 1992).

Every inversion method needs an error vector or objective function to be minimized and, in the present case, the error can be calculated from the equation given below to determine the variation between the observed and calculated anomalies (Kaikkonen and Sharma 1998), thus:

$$\varphi = \frac{1}{N} \sum_{i=1}^{N} \left(\frac{V_i^0 - V_i^c}{|V_i^0| + (V_{max}^0 - V_{min}^0)/2}\right)^2 \tag{2}$$

where N refers to number of data, V_i^0 and V_i^c are the ith observed and model responses, respectively, V_{max}^0 and V_{min}^0 are the maximum and minimum values, respectively, of synthetic/field data.

Moreover, to find a global solution, a single run is not sufficient, and hence in the present case, 10 runs were completed to find the mean model. Next, a Gaussian probability density function (PDF) was
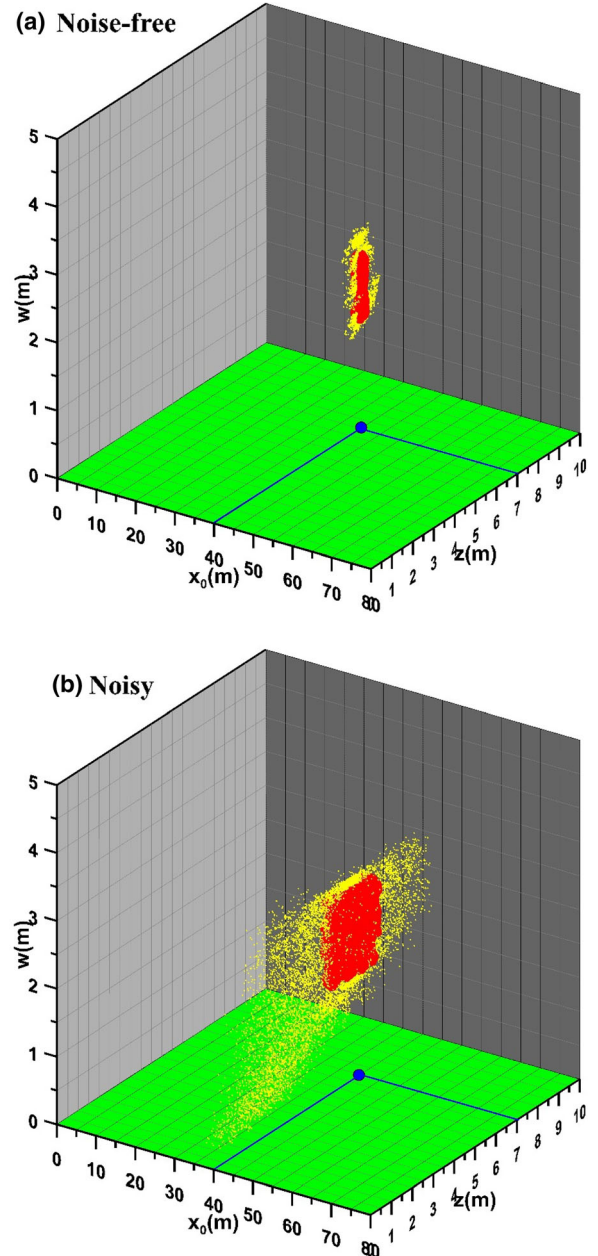

Figure 5. 3D cross-plot for model 1. Yellow points represent true values. Red fields represent uncertainty boundaries and peak PDF range.

calculated to find the most appropriate model and to minimize the uncertainty in the final mean model, which is close to the global mean model. To achieve this, we followed the work of Mosegaard and Tarantola (1995) and Sen and Stoffa (1996). The particulars of the global model, besides uncertainty analysis, can be understood from several works of literature, viz. Biswas (2016, 2018) and Trivedi et al.
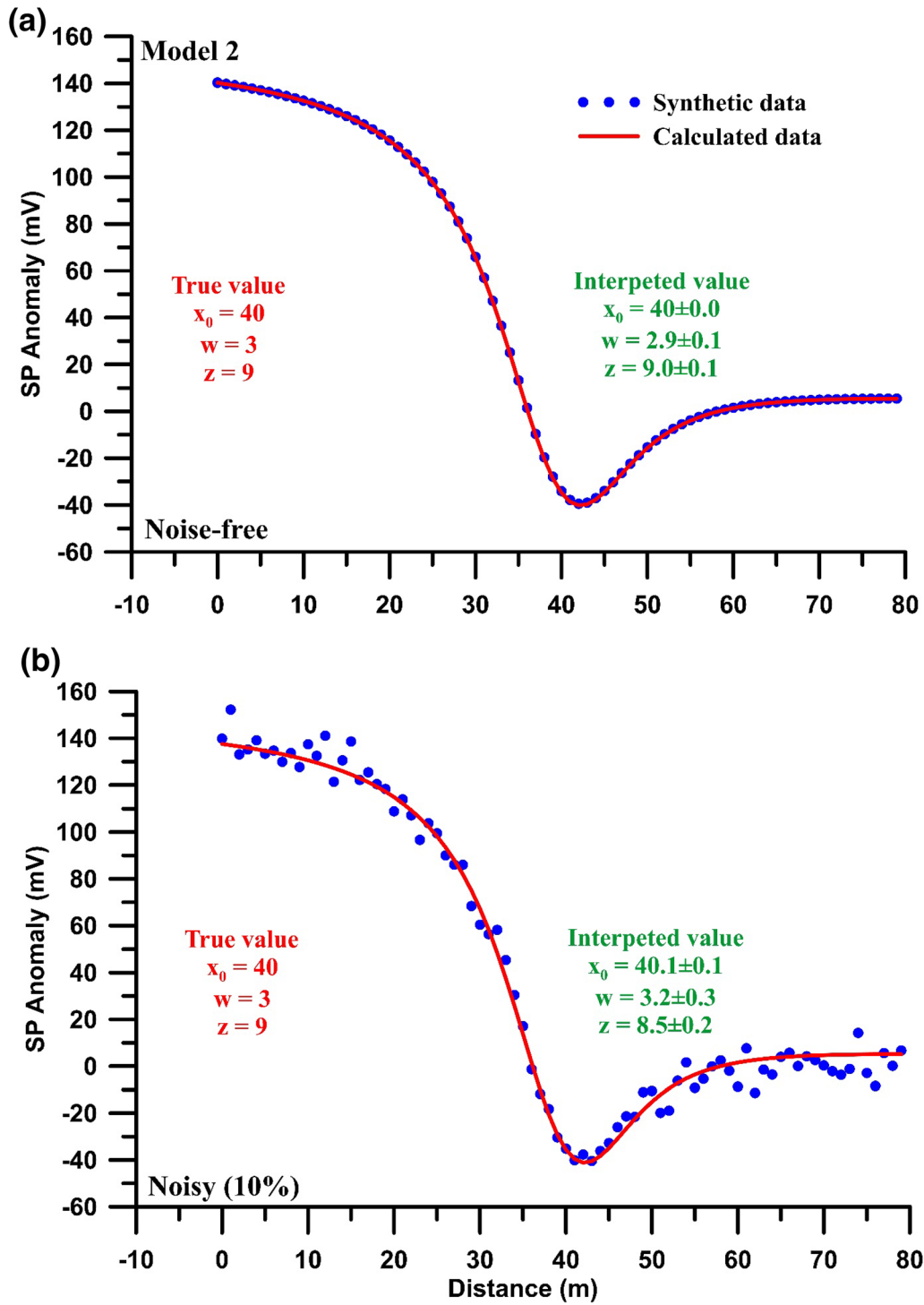
(a)

Model 2

True value
$x_0 = 40$
$w = 3$
$z = 9$

Interpeted value
$x_0 = 40\pm0.0$
$w = 2.9\pm0.1$
$z = 9.0\pm0.1$

Noise-free

• • • Synthetic data
—— Calculated data

SP Anomaly (mV)

Distance: -10 0 10 20 30 40 50 60 70 80

(b)

True value
$x_0 = 40$
$w = 3$
$z = 9$

Interpeted value
$x_0 = 40.1\pm0.1$
$w = 3.2\pm0.3$
$z = 8.5\pm0.2$

Noisy (10%)

SP Anomaly (mV)

Distance (m): -10 0 10 20 30 40 50 60 70 80

Figure 6. Computed response for model 2.

Table 2. Computed parameters for model 2

Parameters	True value	Range	Mean model	
			Noise-free	Noisy
I_1	200	0–250	208.0 ± 12.9	181.9 ± 14.6
I_2	150	0–200	154.3 ± 12.7	133.4 ± 14.1
x_0 (m)	40	0–80	40.0 ± 0.0	40.1 ± 0.1
w (m)	3	0–5	2.9 ± 0.2	3.2 ± 0.3
z (m)	9	0–10	9.0 ± 0.1	8.5 ± 0.2
Error			1.0×10^{-8}	2.0×10^{-3}

(2020), who applied this for interpretation of various geophysical data. The code was implemented using MS FORTRAN Developer studio in Windows 10 platform. The computation of the entire process takes 30 s (not CPU time). The details of the optimization process are shown in Figure 2.

RESULTS

Theoretical Examples

Model 1

A self-potential anomaly was generated, using Eq. (1), for a 2D inclined plate-type structure (Fig. 3a) with different parameters (Table 1). The inversion algorithm developed for such type of structure was applied to interpret the synthetic data. All five parameters for 2D inclined plate-type structures were delineated, and the results are shown in Table 1. Out of five parameters, as mentioned in the theoretical formulation, the important for mineral exploration is the zero-crossing (x_0), half-width (w), and the depth (z). Hence, we tried to study whether inversion can delineate these parameters or not. Next, we tried to study the histogram of x_0, w, and z. We found that x_0 and z show peaks in true values; however, w shows a wide solution (Fig. 4a). This suggests that x_0 and z can be well resolved but there is uncertainty in w. To confirm these observations, we again tried to see a 3D cross-plot analysis between x_0, w, and z. It can be also be seen from the cross-plot that x_0 and z are very close to their true values, but w shows a wide solution (Fig. 5a). However, the elucidated parameters are very close to their true values, which were taken for synthetic analysis, and the parameters (x_0, w, and z) were in-

side the uncertainty boundaries and peak PDF range.

Next, to see the influence of noisy synthetic data, 5% Gaussian noise (i.e., data multiplied by Gaussian random values with mean of 1 and standard deviation of 0.2) was added to the same data and the VFSA procedure was carried out again (Fig. 3b). The inversion algorithm successfully inverted all the parameters. It was found that x_0 and z show peaks of their true values, but w shows a varied array of solutions according to a histogram analysis (Fig. 4b). To confirm this, we again studied the cross-plot and found the same as for the noise-free synthetic data. 5b shows the cross-plot for the noise-corrupted synthetic data. Figure 3a and b shows the responses from synthetic and calculated data. Table 1 shows the interpreted parameters for this model.

Model 2

The second model (Fig. 6a), a 2D inclined plate, was taken to see the variations of w and z. The inversion procedure was executed for this model and the parameters were interpreted. Again, it was found that w shows varied solutions; however, x_0, and z can be determined precisely. Histograms and cross-plots were very similar as for model 1 and hence were not shown here for brevity. Moreover, to check the consistency in higher degree of noise-corrupted data, 10% Gaussian noise was added to this model (Fig. 6b). The inversion procedure was again executed for this model, and the results were the same as discussed for model 1. Table 2 shows the final interpreted parameters, and Figure 6a and b shows the calculated anomalies in case of noise-free and noisy data, respectively.
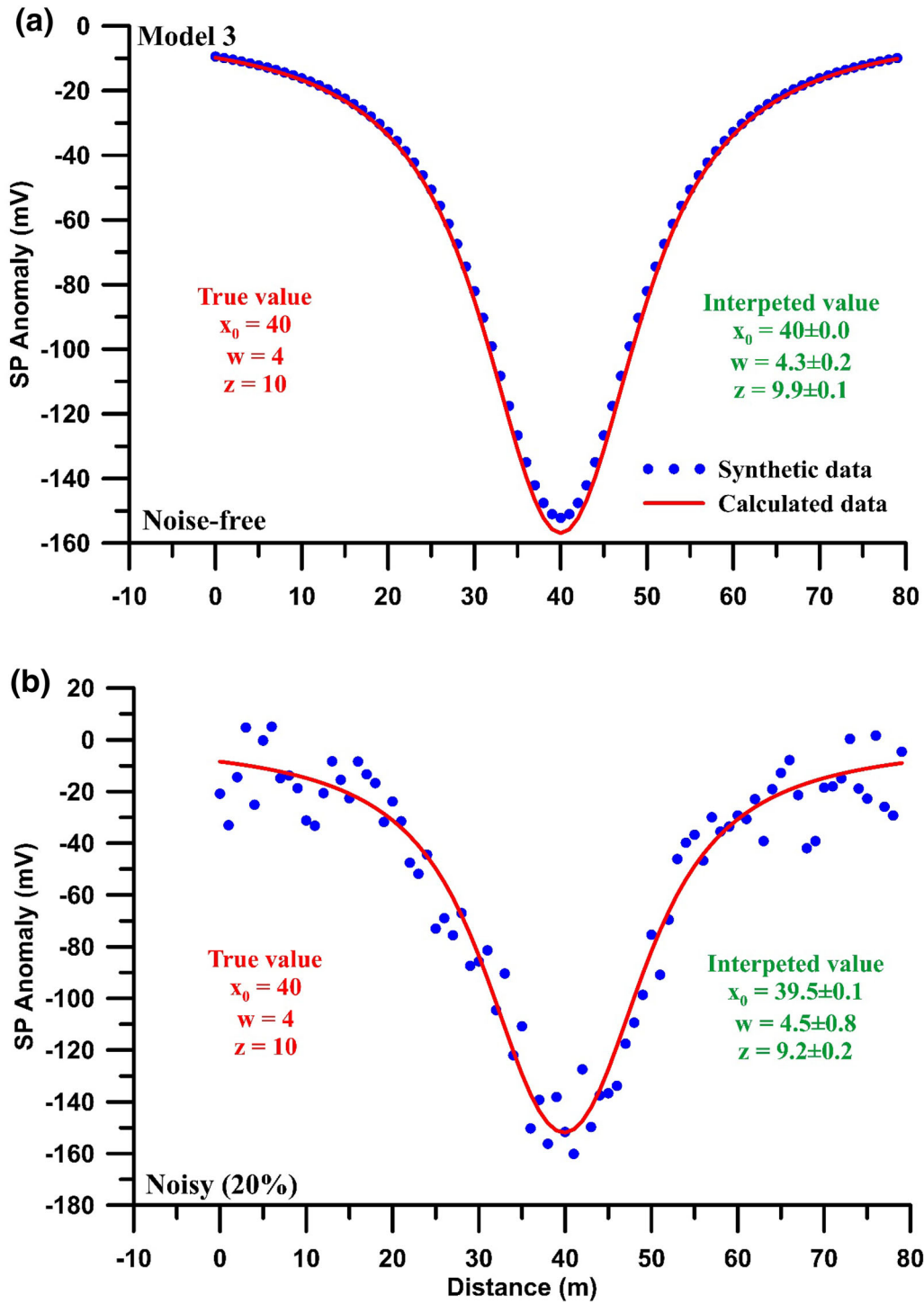
Figure 7. Computed response for model 3.

Table 3. Computed parameters for model 3

Parameters	True value	Range	Mean model	
			Noise-free	Noisy
I_1	200	0–300	189.3 ± 8.7	145.4 ± 33.0
I_2	200	0–300	189.4 ± 8.6	145.3 ± 32.9
x_0 (m)	40	0–80	40.0 ± 0.0	39.5 ± 0.1
w (m)	4	0–10	4.3 ± 0.2	4.5 ± 0.8
z (m)	10	0–20	9.9 ± 0.1	9.2 ± 0.2
Error			1.2×10^{-8}	9.0×10^{-3}
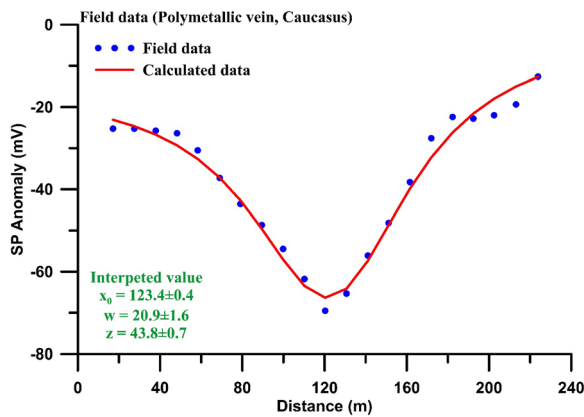
Figure 8. Computed response for field data (polymetallic vein, Caucasus).

Model 3

The third model, a 2D vertical plate-type ($I_1 = I_2$) structure, was taken to see whether it can be interpreted as well by the inversion procedure as a different model (Fig. 7a). The inversion procedure was used to interpret the data and it yielded the same results as for Models 1 and 2. The histograms and cross-plots were found to agree with those of model 1. Moreover, to check whether noisy data for

this model can be interpreted, 20% Gaussian noise was added to the data and the VFSA process was again applied (Fig. 7b). The results were the same as discussed earlier (Table 3). Figure 7 shows the computed responses for both types of data for model 3.

Field Examples

To confirm the usefulness and consistency of the present method, three field examples were used.

Polymetallic Sulfide Deposit

The first example was from a polymetallic vein-type deposit in the Caucasus (after Eppelbaum and Khesin 2012). The anomaly data were digitized at 2.57 m intervals. The data were interpreted by Essa and El-Hussein (2017) considering 2D plate and by Gobashy et al. (2020) considering a 2D inclined sheet-type structure. These field data were again interpreted here using the proposed inversion algorithm. It was found that the important parameters for 2D inclined plate-type structures were depth and half-width. The present results show that the depth of the body was 44 m and half-width 21 m. Figure 8

Table 4. Computed parameters for field example (polymetallic vein, Caucasus)

Parameters	Range	Mean model	Essa and El-Hussein (2017)	Gobashy et al. (2020)
I_1	0–100	60.7 ± 5.3	–	–
I_2	0–110	65.7 ± 5.3	–	–
x_0 (m)	100–140	123.4 ± 0.4	–	211.437^a
w (m)	0–50	20.9 ± 1.6	0.64	–
z (m)	0–50	43.8 ± 0.7	30.7	30.88
Error		2.0×10^{-3}	–	–

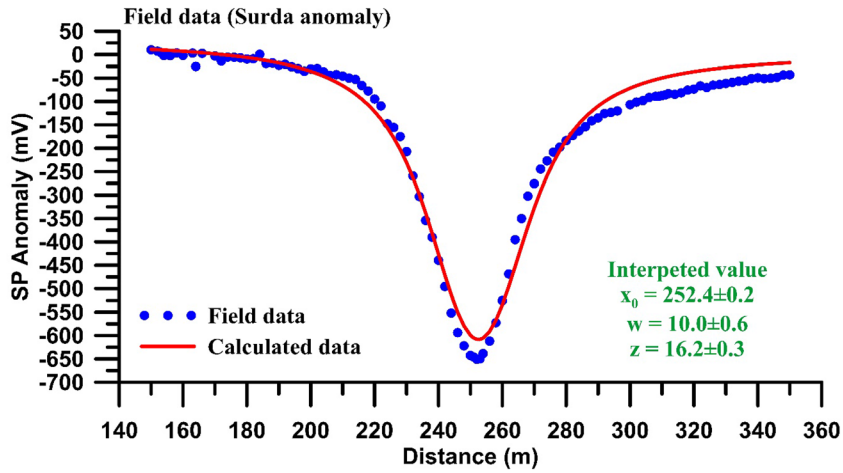[a]x-axis was different in this case

Figure 9. Computed response for field data (Surda anomaly).

Table 5. Computed parameters for field example (Surda anomaly, India)

Parameters	Range	Mean model	Essa and El-Hussein (2017)	Mehanee et al. (2011)	Gobashy et al. (2020)
I_1	0–600	564.8 ± 35.3	–	–	–
I_2	0–700	555.4 ± 33.1	–	–	–
x_0 (m)	230–260	252.4 ± 0.2	–	–	-4.17[a]
w (m)	0–20	10.0 ± 0.6	10.01	9.8	–
z (m)	0–20	16.2 ± 0.3	10.85	9.5	31.29
Error		3.5×10^{-3}	–	–	–

[a]x-axis was different in this case
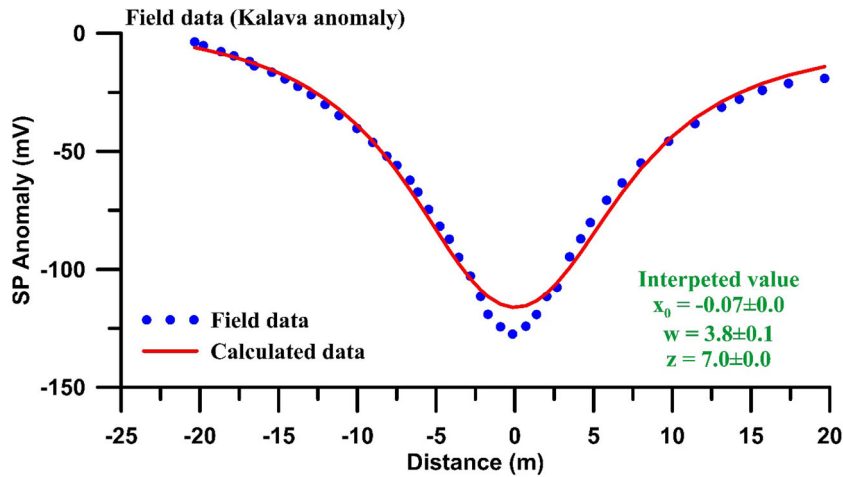
Figure 10. Computed response for field data (Kalava anomaly).
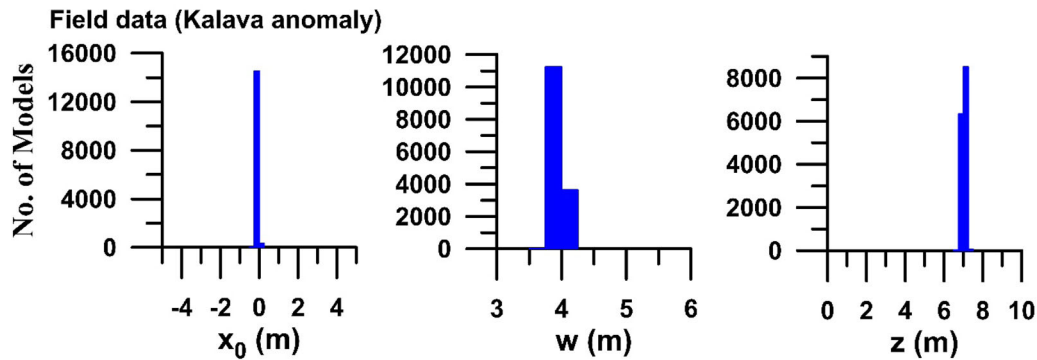
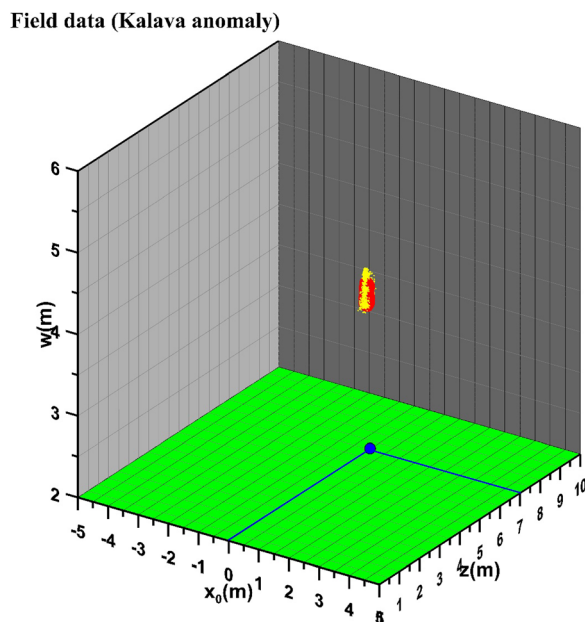**Figure 11.** Histogram analysis for Kalava anomaly.

Figure 12. 3D cross-plot for Kalava anomaly.

shows the responses from the field and calculated data, and Table 4 shows the interpreted parameters.

Surda Anomaly

The second field example was from copper sulfide deposits in the Surda area, India (Murthy and Haricharan 1984; Sundararajan et al. 1998). The data, taken from Sharma and Biswas (2013), have been used widely for interpretation considering 2D

inclined sheet-type subsurface structures (Sundararajan et al. 1998; Sharma and Biswas 2013; Biswas and Sharma 2014b; Biswas 2017; Gobashy et al. 2020). However, the same SP anomaly data were also interpreted considering a 2D inclined plate-type structure (Mehanee et al. 2011; Essa and El-Hussein 2017). The SP data were re-interpreted here considering 2D inclined plate, and the depth and half-width interpreted were 16 m and 10 m, respectively. The interpreted data were consistent with the interpreted depth and half-width from Mehanee et al. (2011) and Essa and El-Hussein (2017). The responses from the field and calculated data are illustrated in Figure 9, and all the interpreted models are shown in Table 5.

Kalava Anomaly

The last field example (Fig. 10) was from a sulfide mineralized deposit in a fault zone in Cuddapah Basin, India (Rao et al. 1982). The data, taken from Biswas and Sharma (2015), were interpreted earlier considering a sheet-type structure (Sundararajan et al. 1990; Jagannadha et al. 1993; Murthy et al. 2005; El-Kaliouby and Al-Garani 2009; Gobashy et al. 2020), a horizontal cylinder-type structure (Biswas and Sharma 2015), a vertical cylinder (Mehanee 2014), and a 2D inclined plate-type structure (Mehanee et al. 2011). The data were re-interpreted here considering a 2D inclined plate-type structure. A histogram was also prepared for these field data to see whether the responses were the same as those found from the synthetic exam-

Table 6. Computed parameters for field example (Kalava anomaly, India)

Parameters	Range	Mean model	Mehanee et al. (2011)	Gobashy et al. (2020)
I_1	0–150	122.3 ± 1.6	–	–
I_2	0–120	119.3 ± 1.6	–	–
x_0 (m)	– 5 to 5	– 0.07 ± 0.0	–	– 0.455
w (m)	0–10	3.8 ± 0.1	2.13	–
z (m)	0–10	7.0 ± 0.0	3.65	7.35
Error		9.0×10^{-4}	–	–

ples. It was found that w also shows a wide range; however, x_0 and z were close to their near probable values (Fig. 11). Moreover, a 3D cross-plot also shows that x_0 and z were very close to the probable values but w widely varies (Fig. 12). The interpreted z and w were 7 m and 3.8 m, respectively. The interpreted depth is consistent with Biswas and Sharma (2015) but somewhat different from Mehanee et al. (2011). Figure 10 shows the computed response, and Table 6 shows the interpreted parameters.

CONCLUSIONS

We have developed an inversion algorithm for the delineation, from self-potential data, of different parameters associated with a 2D plate-type structure. The method of VFSA was applied to determine the 2D plate viz. location of the body (x_0), its half-width (w) and its depth (z). The solutions show that the technique can delineate all the three parameters; however, there some small uncertainty in determining w, which varies widely but within uncertainty limits. Analyses of histograms and cross-plots reveal the same. The technique was verified using noise-free and noisy synthetic data, and it can guess all the three parameters with good accuracy. Three field examples were also interpreted, and the results were consistent with results of other techniques published in the literature. The inversion method can interpret self-potential data considering a 2D inclined plate-type structure without a priori evidence of the sub-surface structure and variation in resistivity data. However, the present method cannot be considered as a final interpretation for mineral exploration; rather, it should be integrated with other geophysical techniques for more reliable results. The method can be used as well for single and/or multiple structures associated with mineralization.

REFERENCES

Abdelazeem, M., Gobashy, M., Khalil, M. H., & Abdraboub, M. (2019). A complete model parameter optimization from self-potential data using Whale algorithm. *Journal of Applied Geophysics, 170,* 103825.

Abdelrahman, E. M., Abdelazeem, M., & Gobashy, M. (2019). A minimization approach to depth and shape determination of mineralized zones from potential field data using the Nelder-Mead simplex algorithm. *Ore Geology Reviews, 114,* 103123.

Abdelrahman, E. M., El-Araby, H. M., Hassanein, A. G., & Hafez, M. A. (2003). New methods for shape and depth determinations from SP data. *Geophysics, 68,* 1202–1210.

Abdelrahman, E. M., Hassaneen, A Gh, & Hafez, M. A. (1998). Interpretation of self-potential anomalies over two-dimensional plates by gradient analysis. *Pure and Applied Geophysics, 152,* 773–780.

Abdelrahman, E. M., & Sharafeldin, M. S. (1997). A least-squares approach to depth determination from self-potential anomalies caused by horizontal cylinders and spheres. *Geophysics, 62,* 44–48.

Asfahani, J., & Tlas, M. (2005). A constrained nonlinear inversion approach to quantitative interpretation of self-potential anomalies caused by cylinders, spheres and sheet-like structures. *Pure and Applied Geophysics, 162,* 609–624.

Biswas, A. (2013). Identification and resolution of ambiguities in interpretation of self-potential data: Analysis and integrated study around South Purulia Shear Zone, India. Ph.D. thesis, Department of Geology and Geophysics, Indian Institute of Technology Kharagpur, 199 pp. Retrieved May, 2020 from http://www.idr.iitkgp.ac.in/xmlui/handle/123456789/3247.

Biswas, A. (2016). A comparative performance of least square method and very fast simulated annealing global optimization method for interpretation of Self-Potential anomaly over 2-D inclined sheet type structure. *Journal of the Geological Society of India, 88*(4), 493–502.

Biswas, A. (2017). A review on modeling, inversion and interpretation of self-potential in mineral exploration and tracing Paleo-Shear zones. *Ore Geology Reviews, 91,* 21–56.

Biswas, A. (2018). Inversion of source parameters from magnetic anomalies for mineral/ore deposits exploration using global optimization technique and analysis of uncertainty. *Natural Resources Research, 27*(1), 77–107.

Biswas, A. (2019). Inversion of amplitude from the 2-D analytic signal of self-potential anomalies. In K. Essa (Ed.), *Minerals* (pp. 13–45). London: In-Tech Education and Publishing.

Biswas, A., & Sharma, S. P. (2014a). Resolution of multiple sheet-type structures in self-potential measurement. *Journal of Earth System Science, 123*(4), 809–825.

Biswas, A., & Sharma, S. P. (2014b). Optimization of Self-Potential interpretation of 2-D inclined sheet-type structures based on Very Fast Simulated Annealing and analysis of ambiguity. *Journal of Applied Geophysics, 105,* 235–247.

Biswas, A., & Sharma, S. P. (2015). Interpretation of self-potential anomaly over idealized body and analysis of ambiguity using very fast simulated annealing global optimization. *Near Surface Geophysics, 13*(2), 179–195.

Biswas, A., & Sharma, S. P. (2016). Integrated geophysical studies to elicit the structure associated with Uranium mineralization around South Purulia Shear Zone, India: A Review. *Ore Geology Reviews, 72,* 1307–1326.

Biswas, A., & Sharma, S. P. (2017). Interpretation of Self-potential anomaly over 2-D inclined thick sheet structures and analysis of uncertainty using very fast simulated annealing global optimization. *Acta Geodaetica et Geophysica, 52*(4), 439–455.

Di Maio, R., Piegari, E., Rani, P., & Avella, A. (2016a). Self-Potential data inversion through the integration of spectral analysis and tomographic approaches. *Geophysical Journal International, 206,* 1204–1220.

Di Maio, R., Rani, P., Piegari, E., & Milano, L. (2016b). Self-potential data inversion through a Genetic-Price algorithm. *Computers & Geosciences, 94,* 86–95.

Dmitriev, A. N. (2012). Forward and inverse self-potential modeling: A new approach. *Russian Geology and Geophysics, 53,* 611–622.

El-Kaliouby, H. M., & Al-Garani, M. A. (2009). Inversion of self-potential anomalies caused by 2D inclined sheets using neural networks. *Journal of Geophysics and Engineering, 6,* 29–34.

Eppelbaum, L., & Khesin, B. (2012). Methodological specificities of geophysical studies in the complex environments of the caucasus. In L. Eppelbaum & B. Khesin (Eds.), *Geophysical studies in the caucasus* (pp. 39–138). Berlin: Springer.

Essa, K. S. (2011). A new algorithm for gravity or self-potential data interpretation. *Journal of Geophysics and Engineering, 8,* 434–446.

Essa, K. S., & El-Hussein, M. (2017). A new approach for the interpretation of self-potential data by 2-D inclined plate. *Journal of Applied Geophysics, 136,* 455–461.

Essa, K., Mahanee, S., & Smith, P. D. (2008). A new inversion algorithm for estimating the best fitting parameters of some geometrically simple body to measured self-potential anomalies. *Exploration Geophysics, 39,* 155–163.

Gobashy, M., Abdelazeem, M., Abdrabou, M., & Khalil, M. H. (2020). Estimating model parameters from self-potential anomaly of 2D inclined sheet using whale optimization algorithm: Applications to mineral exploration and tracing shear zones. *Natural Resources Research, 29,* 499–519.

Göktürkler, G., & Balkaya, Ç. (2012). Inversion of self-potential anomalies caused by simple geometry bodies using global optimization algorithms. *Journal of Geophysics and Engineering, 9,* 498–507.

Hafez, M. A. (2005). Interpretation of the self-potential anomaly over a 2D inclined plate using a moving average window curves method. *Journal of Geophysics and Engineering, 2,* 97–102.

Ingber, L., & Rosen, B. (1992). Genetic algorithms and very fast simulated reannealing: A comparison. *Mathematical and Computer Modeling, 16*(11), 87–100.

Jagannadha, R. S., Rama, R. P., & Radhakrishna, M. I. V. (1993). Automatic inversion of self-potential anomalies of sheet-like bodies. *Computers & Geosciences, 19,* 61–73.

Jardani, A., Revil, A., Boleve, A., & Dupont, J. P. (2008). Three-dimensional inversion of self-potential data used to constrain the pattern of groundwater flow in geothermal fields. *Journal of Geophysical Research-Solid Earth, 113,* B09204.

Kaikkonen, P., & Sharma, S. P. (1998). 2-D nonlinear joint inversion of VLF and VLF-R data using simulated annealing. *Journal of Applied Geophysics, 39,* 155–176.

Kulessa, B., Hubbard, B., & Brown, G. H. (2003). Cross-coupled flow modeling of coincident streaming and electrochemical potentials and application to sub-glacial self-potential data. *Journal of Geophysical Research, 108*(B8), 2381.

Lile, O. B. (1994). Modeling self-potential anomalies from electric conductors. In *EAGE 56th meeting and technical exhibition* (Vienna, Austria).

Mehanee, S. (2014). An efficient regularized inversion approach for self-potential data interpretation of ore exploration using a mix of logarithmic and non-logarithmic model parameters. *Ore Geology Reviews, 57,* 87–115.

Mehanee, S. (2015). Tracing of paleo-shear zones by self-potential data inversion: case studies from the KTB, Rittsteig, & Grossensees graphite-bearing fault planes. *Earth, Planets and Space, 67,* 14–47.

Mehanee, S., Essa, K. S., & Smith, P. D. (2011). A rapid technique for estimating the depth and width of a two-dimensional plate from self-potential data. *Journal of Geophysics and Engineering, 8,* 447–456.

Mendonca, C. A. (2008). Forward and inverse self-potential modeling in mineral exploration. *Geophysics, 73,* F33–F43.

Monteiro Santos, F. A. (2010). Inversion of self-potential of idealized bodies anomalies using particle swarm optimization. *Computers & Geosciences, 36,* 1185–1190.

Mosegaard, K., & Tarantola, A. (1995). Monte Carlo sampling of solutions to inverse problems. *Journal of Geophysical Research, 100*(B7), 12431–12447.

Murthy, B. V. S., & Haricharan, P. (1984). Self-potential anomaly over double line of poles—interpretation through log curves. *Proceedings Indian Academy of Science (Earth and Planetary Science), 93,* 437–445.

Murthy, B. V. S., & Haricharan, P. (1985). Nomograms for the complete interpretation of spontaneous potential profiles over sheet like and cylindrical 2D structures. *Geophysics, 50,* 1127–1135.

Murthy, I. V. R., Sudhakar, K. S., & Rao, P. R. (2005). A new method of interpreting self-potential anomalies of two-dimensional inclined sheets. *Computers & Geosciences, 31,* 661–665.

Paul, M. K. (1965). Direct interpretation of self-potential anomalies caused by inclined sheets of infinite extension. *Geophysics, 30,* 418–423.

Paul, M. K., Data, S., & Banerjee, B. (1965). Interpretation of SP anomalies due to localized causative bodies. *Pure and Applied Geophysics, 61,* 95–100.

Rao, A. D., Babu, H., & SivakumarSinha, G. D. (1982). A Fourier transform method for the interpretation of self-potential

anomalies due to two-dimensional inclined sheet of finite depth extent. *Pure and Applied Geophysics, 120,* 365–374.

Rao, B. S. R., Murthy, I. V. R., & Reddy, S. J. (1970). Interpretation of self-potential anomalies of some simple geometrical bodies. *Pure and Applied Geophysics, 78,* 60–77.

Rothman, D. H. (1985). Nonlinear inversion, statistical mechanics and residual statics estimation. *Geophysics, 50,* 2784–2796.

Rothman, D. H. (1986). Automatic estimation of large residual statics correction. *Geophysics, 51,* 337–346.

Roudsari, M. S., & Beitollahi, A. (2013). Forward modeling and inversion of self-potential anomalies caused by 2D inclined sheets. *Exploration Geophysics, 44,* 176–184.

Roudsari, M. S., & Beitollahi, A. (2015). Laboratory modelling of self-potential anomalies due to spherical bodies. *Exploration Geophysics, 46,* 320–331.

Roy, S. V. S., & Mohan, N. L. (1984). Spectral interpretation of self-potential anomalies of some simple geometric bodies. *Pure and Applied Geophysics, 78,* 66–77.

Sato, M., & Mooney, H. M. (1960). The electrochemical mechanism of sulfide self-potentials. *Geophysics, 25,* 226–249.

Sen, M. K., & Stoffa, P. L. (1996). Bayesian inference, Gibbs sampler and uncertainty estimation in geophysical inversion. *Geophysical Prospecting, 44,* 313–350.

Sen, M. K., & Stoffa, P. L. (2013). *Global optimization methods in geophysical inversion* (2nd ed.). London: Cambridge Publisher.

Sharma, S. P. (2012). VFSARES—A very fast simulated annealing FORTRAN program for interpretation of 1-D DC resistivity sounding data from various electrode array. *Computers & Geosciences, 42,* 177–188.

Sharma, S. P., & Biswas, A. (2013). Interpretation of self-potential anomaly over 2D inclined structure using very fast simulated annealing global optimization–An insight about ambiguity. *Geophysics, 78*(3), WB3–WB15.

Sundararajan, N., Arun Kumar, I., Mohan, N. L., & SeshagiriRao, S. V. (1990). Use of Hilbert transform to interpret self-potential anomalies due to two dimensional inclined sheets. *Pure Applied Geophysics, 133,* 117–126.

Sundararajan, N., Srinivasa Rao, P., & Sunitha, V. (1998). An analytical method to interpret self-potential anomalies caused by 2D inclined sheets. *Geophysics, 63,* 1551–1555.

Tlas, M., & Asfahani, J. (2007). A best-estimate approach for determining self-potential parameters related to simple geometric shaped structures. *Pure and Applied Geophysics, 164,* 2313–2328.

Tlas, M., & Asfahani, J. (2013). An approach for interpretation of self-potential anomalies due to simple geometrical structures using flair function minimization. *Pure and Applied Geophysics, 170,* 895–905.

Trivedi, S., Kumar, P., Parija, M. P., & Biswas, A. (2020). Global optimization of model parameters from the 2-D analytic signal of gravity and magnetic anomalies. In A. Biswas & S. P. Sharma (Eds.), *Advances in modeling and interpretation in near surface geophysics* (pp. 189–221). Berlin: Springer.